Turning the Muroto seafloor cable into a long DAS sensing array

Martin Karrenbach(1), Rob Ellwood(1), Victor Yartsev(1), Steve Cole(1), Eiichiro Araki(2), Toshinori Kimura(2) and Hioryuki Matsumoto(2)

(1) *OptaSense*, (2) *JAMSTEC*

Abstract: Unused existing submarine cables containing standard telecom fiber for data transmission can efficiently be turned into seismic sensing arrays. We demonstrate a case where a 120km long submarine cable provided a 50km long distributed fiber-optic sensing array. The Muroto Cable originates in the landing station near Cape Muroto, Japan, and extends offshore from there. It provides power and data transmission to distant seafloor observatories. An active source seismic data set was acquired with fiber-optic DAS sensing technology. Clear signals from an airgun source were recorded over the entire sensing array for source-receiver offsets up to 100 kilometers. Passive seismic data (earthquakes) were also recorded. Location consistent variations in strain sensing amplitudes due to seafloor coupling were observed, indicating spatial variability of ground/seafloor coupling. We analyze source and receiver consistent effects that are induced by cable construction and seafloor conditions as evidenced by weak and strong coupling regions along the sensing array. We observe direct, reflected, refracted and mode-converted arrivals allowing analysis on various spatial scales.We show that legacy power and data transmission cables, such as for offshore oil and gas infrastructure, trans-oceanic data transmission, or connection to other offshore infrastructure, can be used to acquire high-quality seismic data. The study also provides insight into the design and installation of new dedicated seafloor cable sensing arrays.

DOI:10.1190/segj2021-002.1

1. Introduction

Existing seafloor cables provide an opportunity to conduct seismic surveys without the need to deploy ocean-bottom seismometers or towed streamer arrays. Seafloor fiber-optic cables are widely installed for a variety of purposes. In this instance they provide power and data transmission capabilities for existing seafloor devices as part of a scientific seafloor observatory (Fujiwara et al, 1998; Lindsey et al, 2019).

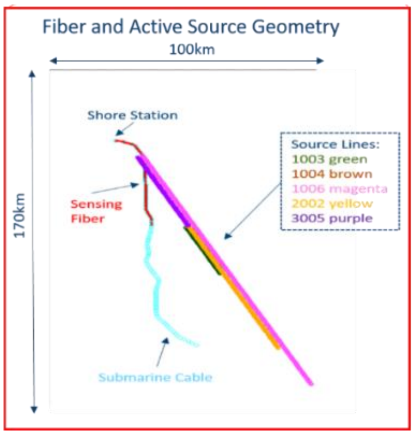

Figure 1: Map of the survey area offshore Japan, with detail of the fiber optic cable geometry and airgun source profiles. The sensing array is shown in red, while the full cable extent is in blue.

In November 2019, we collected DAS data on such a fiber near Muroto, Japan, recording an active-source airgun survey (Fig.1) as well as ambient seismic data including several earthquakes. Although the fiber was installed over twenty years earlier, good signal quality was observed over the entire length of the array.

2. Data Acquisition

The DAS system acquired data for 5 days in continuous mode covering periods of active airgun shots and ambient noise recording. The sensor channels were spaced 1m apart and a temporal sampling rate of 500Hz was used. The primary gauge length selected for this data set was 34m. This provided the greatest resolution while maintaining sensitivity. Thus, the 50000 channels of the DAS system produced a sensing array of 50 km extent, covering about half of physically available length of the 120 km fiber cable. Active shot gathers were recorded for over 1400 source locations along multiple parallel lines with an approximate nominal shot spacing of 200m.

3. Active Source Consistency

A single strain-recording shot gather is shown in Figure 2 as an example. The source is located 22 km from the start of the fiber and illuminates the entire sensing array. It is representative of the data quality achieved throughout the survey.

The short-wavelength strain response in the near shore region (first 2.4 km) dominates on the left. On the right towards the far off-shore channels we see long-wavelength signals. These are likely caused by subsea currents and wave action imparting strain and temperature changes onto the seafloor cable.

The airgun creates hydro-acoustic and strain signals in a higher frequency range (here typically up to 30-40 Hz). These direct arrivals are strong in the vicinity of the source location and diminish with offset. Refractions along the seafloor and from deeper subsurface layers arrive first at longer offsets. At various offsets the reflected, scattered and converted waves are all recorded strongly since their wave field motion aligns with the axial strain component direction within the fiber.

In addition to the wave field Figure 2 shows also the various fiber-optic cable types that are present on the seafloor. These cable types contain different armouring in order to survive the harsh seafloor conditions. In general, the different cable constructions do not impact the recorded seismic wave field amplitude and SNR significantly.

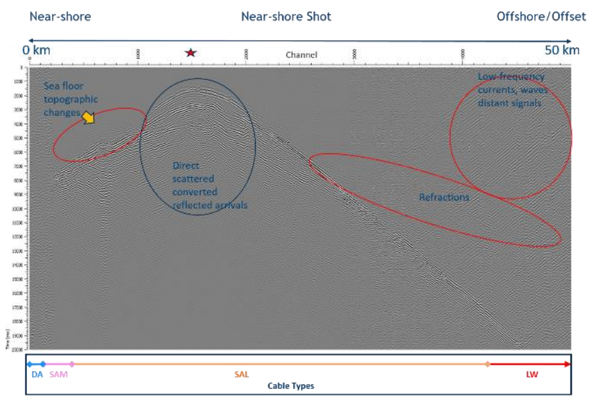

Figure 2: Near-shore airgun shot gather covering 50km lateral sensing distance and 20 seconds of time duration.

Seismic traces at various source offsets are displayed as a common receiver gather in Figure 3. The hyperbolic near-source-offset wave field response is coherent and shows consistent arrival time moveout. At larger source offsets the refracted waves dominate. Thus, direct, reflected, mode-converted and far-offset refracted energy arrive in the sensing array over the entire source offset range of about 38km.

In Figure 4 we focus on a few sources over a source offset range of 4 km and see consistent behaviour in the near and far field regions. Besides wave propagation effects the amplitudes are mainly influenced by the airgun source radiation pattern as well as the receiver cable sensitivity directivity pattern. At this receiver location the fiber-optic cable is well coupled to the seafloor, thus the strain wave field is transferred reliably to the optical fiber.

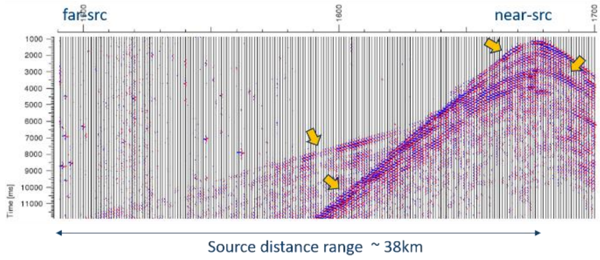

Figure 3: Common receiver gather with a maximum shot offset of 38 km. Signatures are consistent. The recordings combine source directivity and receiver sensitivity characteristics.

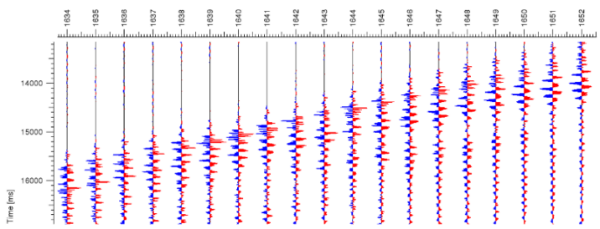

Figure 4: Source signature details for source locations nominally 200 m apart over a range of 4 km. Consistency is maintained in near and far field regions.

4. Receiver Location Consistent Effects

While cable type/construction can cause small strain amplitude effects, the local site dependent effects can significantly impact the recorded strain amplitude. In this data set we observe that the receiver sensitivity correlates strongly with variable coupling induced by local site-dependent effects. This behavior is consistent for active source and ambient noise recordings.

We computed the recorded RMS energy level over all sources and time periods for each receiver location in order to characterize the overall behavior of each sensor. Thus, we average out impacts due to seafloor environmental changes over the course of the survey. Figure 5 shows the amplitudes on a logarithmic scale for each receiver location from 0 to 50 km. For the first 2 km, which coincides with the heavily armoured cable variant, the strain is dominated by the near shore waves and currents. Once the cable reaches the seafloor at 800 m depth the strain energy levels drop and undulate around a central level. Here we observe receiver location consistent effects that do not vary over time or with incident wave fields. However, we

DOI:10.1190/segj2021-002.1

DOI:10.1190/segj2021-002.1

observe that these location consistent coupling variations extend over various spatial scales. In this data set, along the Muroto Cable, the low-sensitivity (low-coupling) regions typically extend over 10's to 100's of meters.

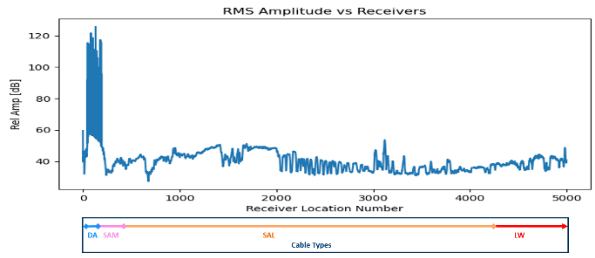

Figure 5: RMS energy integrated over all sources and time periods shows receiver location consistent amplitude level changes over the 50km range. These variations are likely due to variations in seafloor coupling. Receiver amplitudes are ploted every 10 meters.

In Figure 6-8, we examine the amplitude behavior at two specific channel locations 28805 and 29905 (meters) over a 3 second time window. While the first location (28805 m +/- 125m) in Figure 6 exhibits good seafloor coupling, the second (29905 m +/-80m) is much weaker.

5. Weak and Strong Coupling

The well-coupled region shows consistent amplitude, while the poorly-coupled region registers lower source generated wave field amplitudes, and show additional high-frequency strain responses with very high apparent velocity, that are uncorrelated to the source generated arrivals.

The superimposed strain responses are illustrated further in Figures 7 and 8. Since we record with a dense receiver spacing we are able to process the data on a fine scale utilizing array-processing techniques. Figure 7 applies a plane wave decomposition to the strong and weak coupling regions independently. Figure 7 on the left displays the phase slowness over a 5 second time window within the strong coupling region. It captures the main source generated arrivals around 5 seconds. The gray scale indicates a strong relative energy at a phase velocity of 0.0005 s/m, corresponding to the modestly dipping low-frequency arrival band. The energy peak values are indicated in red color.

The plane wave decomposition in the strong (left) and weak (right) coupling regions exhibit overall consistency. However, the weak region shows a small time delay due to the true first arrival phase being very weak, and thus being dominated by the second arrival phase.

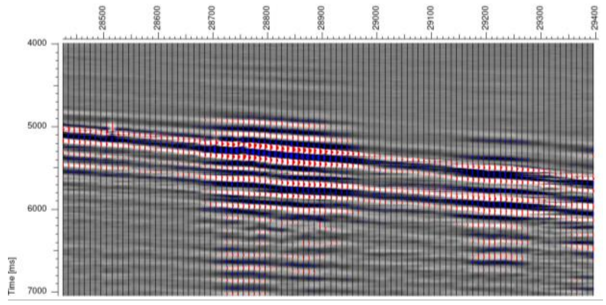

Figure 6: Site dependent sensitivity, amplitude and frequency changes over a short lateral distance. Wiggle traces are overlaid on the grayscale plot to visually emphasize the amplitude variations.

The larger slowness extent is likely due to elevated higher frequency waves being induced by the source generated arrival phases. In particular, near the zero slowness we observe energy being present. However, the energy levels in both (strong and weak coupling) scenarios differ by about two orders of magnitude.

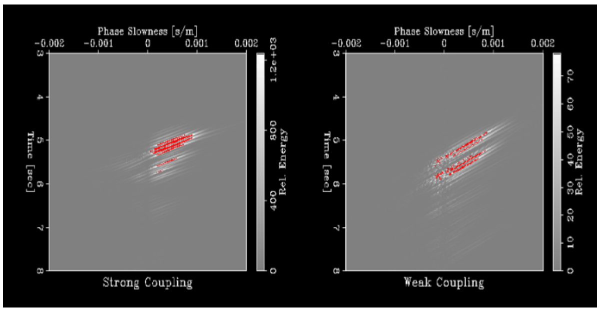

Figure 7: Plane wave decomposition in the strong (left) and weak (right) coupling regions show overall consistency. However, the weak region covers a larger slowness range due to higher frequencies being induced.

In Figure 8 we analyze the weakly coupled section further. Considering the high-frequency nature observed for the arrivals in Figure 6, we proceeded to plane-wave decompose low and high frequency bands separately. Figure 8 left shows the decomposition of the low-frequency wave field up to 30 Hz. It is consistent in dip and arrival time with Figure 7 left – proving to us that the source generated arrivals are mainly contained in this low frequency band.

Figure 8 on the right shows the plane wave decomposition of the 30 Hz high-pass filtered data. For this wave field subset the plane wave content is centered around zero slowness. In addition there is small time delay, when compared to the low-frequency source generated arrivals. The time delay of 0.15s amounts roughly to the time difference of the first and second arrival phase in Figure 7. The weak coupling regions respond mainly to the second and subsequent arrival phases in both low and high frequencies, and the high frequency response above 30 Hz is induced by the low-frequency arrival.

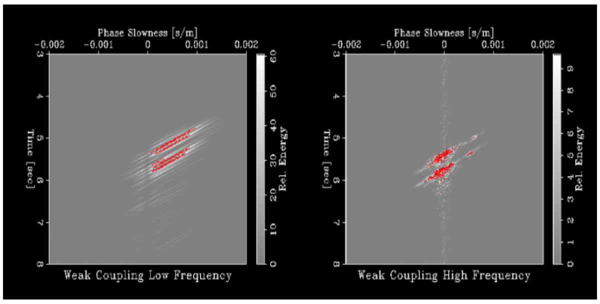

Figure 8: Plane wave decompositions in the weakly coupled region. Left shows 0-30Hz wave field, right shows 30 Hz high-pass wave field with it different dip and timing response.

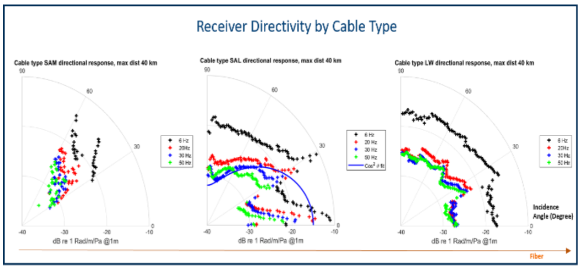

Figure 9: Receiver radiation patterns obtained from data on cable types SAM (left), SAL (middle) and LW (right). The sensitivity is frequency dependent: 6Hz (black), 20 Hz (red), 30Hz (blue) and 50Hz (green). Theoretical $\cos^2$ dependence is shown as a solid blue curve.

6. Receiver Angular Sensitivity

Various cable constructions transduct pressure and strain signals from the environment in different manners, as shown in Figure 9. Arrival amplitudes in various frequency bands were determined from three common receiver gathers utilizing a single source line. The different colors indicate the various frequency band results. The amplitudes are corrected for spherical spreading. For lower frequencies, the broadside null is less pronounced than for higher frequencies. In the 30-90 degree range frequencies above 20 Hz follow the theoretical $\cos^2$ pattern more closely.

7. Conclusions

With minimal effort we are able to turn the Muroto Cable into a long and dense strain sensing array by utilizing a novel DAS interrogator. The DAS system provides long-range, large-aperture and dense spatial and temporal sampling. The DAS system is housed on-shore while interrogating the seafloor fiber-optic cable with 50000 sensing channels over a range of 50km offshore.

This DAS data acquisition successfully collected active and passive data on the Muroto Cable offshore Japan, observing wave mode arrivals on various spatial scales. Utilizing direct wave field arrivals from a controlled airgun source we estimated airgun source consistency, analyzed local site effects and the cable's sensing directionality pattern. All those quantities are important for further detailed data processing and subsurface imaging.

This proof of concept survey demonstrates that legacy power and data transmission cables for offshore oil and gas infrastructure, trans-oceanic data transmission, or connection to other offshore infrastructure can be used to acquire high-quality seismic data. This study also provides insight into the design and installation of new dedicated seafloor cable sensing arrays.

Acknowledgements

We thank JAMSTEC and OptaSense for supporting this research, and for permission to publish the results.

References

Fujiwara, N., Momma, H., Kawaguchi, H., Iwase, R. and Kinoshita, H., 1998, Comprehensive deep seafloor monitoring system in JAMSTEC, Proceedings of 1998 International Symposium on Underwater Technology, Tokyo, Japan, 1998, pp. 383-388, https://doi.org/10.1109/UT.1998.670132

Matsumoto, H., Araki, E., Kimura, T., Fujie, G., Shirashi, K., Tonegawa, T., Obana, K., Arai, R., Kaiho, Y., Nakamura, Y, Yokobiki, T., Kodaira, S. Takahashi, N., Ellwood, R. Yartsev, V. and Karrenbach, M. 2021 Detection of hydroacoustic signals on a fiber-optic submarine cable, Scientific Reports, 2797, Vol 11, Issue 1. https://doi.org/10.1038/s41598-021-82093-8

Williams, E.F., Fernandez-Ruiz, M.R., Magahaes, R., Vanthillo, R., Zhan, Z., Gonzalez-Herraez, M., Martins, H.F, 2019, Distributed sensing of microseisms and teleseisms with submarine dark fiber, Nature communications, 10 (1), 1-11.

Lindsey, N.J., Dawe, T.C., Ajo-Franklin, J.B, 2019, Illuminating sea floor faults and ocean dynamics with dark fiber distributed acoustic sensing, Science, Vol. 366, Issue 6469, 1103-1107.

DOI:10.1190/segj2021-002.1